

Weak charge and weak radius of ^{12}C

Oleksandr Koshchii^{a,*}, Jens Erler^{a,b,c}, Mikhail Gorchtein^d, Charles J. Horowitz^e,
Jorge Piekarewicz^f, Xavier Roca-Maza^g, Chien-Yeah Seng^h, Hubert Spiesberger^a

^a*PRISMA⁺ Cluster of Excellence, Institut für Physik,
Johannes Gutenberg-Universität, D-55099 Mainz, Germany*

^b*Helmholtz Institute Mainz, Johannes Gutenberg-Universität, D-55099 Mainz, Germany*

^c*Departamento de Física Teórica, Instituto de Física,
Universidad Nacional Autónoma de México, 04510 CDMX, México*

^d*PRISMA⁺ Cluster of Excellence, Institut für Kernphysik,
Johannes Gutenberg-Universität, D-55099 Mainz, Germany*

^e*Center for Exploration of Energy and Matter and Department of Physics,
Indiana University, Bloomington, Indiana 47405, USA*

^f*Department of Physics, Florida State University, Tallahassee, Florida 32306, USA*

^g*Dipartimento di Fisica, Università degli Studi di Milano, Via Celoria 16, I-20133 Milano, Italy
and INFN, Sezione di Milano, Via Celoria 16, I-20133 Milano, Italy*

^h*Helmholtz-Institut für Strahlen- und Kernphysik and Bethe Center for Theoretical Physics,
Universität Bonn, D-53115 Bonn, Germany*

(Dated: August 13, 2020)

We present a feasibility study of a simultaneous sub-percent extraction of the weak charge and the weak radius of the ^{12}C nucleus using parity-violating electron scattering, based on a largely model-independent assessment of the uncertainties. The corresponding measurement is considered to be carried out at the future MESA facility in Mainz with $E_{\text{beam}} = 155$ MeV. We find that a combination of a 0.3% precise measurement of the parity-violating asymmetry at forward angles with a 10% measurement at backward angles will allow to determine the weak charge and the weak radius of ^{12}C with 0.4% and 0.5% precision, respectively. These values could be improved to 0.3% and 0.2% for a 3% backward measurement. This experimental program will have impact on precision low-energy tests in the electroweak sector and nuclear structure.

Precise measurements of the parameters of the standard model (SM) are among the main tools to search for or constrain hypothetical contributions from physics beyond the SM. The central parameter of the electroweak sector of the SM is the weak mixing angle θ_W describing the mixing of the SU(2) and U(1) gauge boson fields, which results in the emergence of the physical fields, the massless photon and the massive Z^0 . Its sine squared, $\sin^2\theta_W$, is related to the vector charge of SM fermions with respect to the weak neutral current and can be accessed in various processes and at different energy scales: from Z -pole measurements at colliders [1, 2], including the LHCb [3], ATLAS [4] and CMS [5] experiments, to deep inelastic scattering with electrons [6, 7] and neutrinos [8], to parity violation in atoms [9, 10] and to parity-violating electron scattering (PVES) off protons [11] and electrons [12]. To connect these measurements across the relevant energy scales, the SM running at the one-loop level needs to be taken into account [13, 14]. Currently, this running is theoretically known at the relative level of $\sim 8 \times 10^{-5}$, which provides the basis for an ambi-

tious experimental program at low energies: an ongoing effort in atomic parity violation [15, 16] has the goal to measure the weak charges of heavy nuclei and chains of nuclear isotopes at the per mille precision. The Qweak experiment [11] has recently extracted $\sin^2\theta_W$ from low-energy PVES to 0.5% accuracy. P2@MESA [17] and the MOLLER Collaboration [18] aim at improving that result by factors of 4 and 6, respectively. Further plans involve deep-inelastic electron scattering with SOLID [19].

Apart from tests of the SM, PVES has also been used to address aspects of nucleon and nuclear structure that are elusive to photons. PVES off heavy nuclei with a neutron excess is used to determine the neutron skin [20]—the difference in the radii of the neutron and proton distributions—with the goal of constraining the equation of state (EOS) of neutron rich matter [21]. The lead (Pb) Radius EXperiment (PREX) [22] has provided the first model-independent evidence in favor of a neutron-rich skin in ^{208}Pb [23]. Further experiments with an improved precision are presently being analyzed [24], running [25], or planned [17]. PVES off the proton and light nuclei

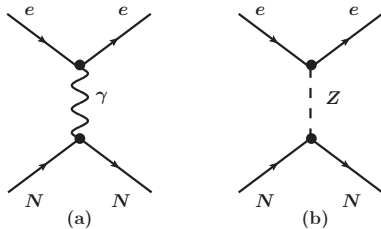


FIG. 1. (a) One-photon exchange and (b) Z^0 exchange diagrams.

has been extensively used to determine the strange quark content of the nucleon [26].

In this Rapid Communication, we consider the parity-violating asymmetry which is defined as the difference between the cross sections for elastic scattering of longitudinally polarized electrons off an unpolarized target,

$$A^{\text{PV}} = \frac{\sigma_R - \sigma_L}{\sigma_R + \sigma_L}, \quad (1)$$

where σ_R (σ_L) stands for the cross section with right-handed (left-handed) electron polarization. The asymmetry arises from the interference between the amplitudes due to the exchange of a virtual photon and the corresponding one for a virtual Z^0 boson as shown in Fig. 1. By conveniently factoring out the Fermi constant G_F , the fine-structure constant α , the four-momentum transfer squared Q^2 , and the ratio of the weak, Q_W , to the electric, Z , nuclear charge, the PV asymmetry for a spinless nucleus consisting of Z protons and N neutrons takes the following form:

$$A^{\text{PV}} = -\frac{G_F Q^2}{4\sqrt{2}\pi\alpha} \frac{Q_W}{Z} (1 + \Delta), \quad (2)$$

where a plane-wave Born (“tree-level”) approximation was assumed. The weak nuclear charge is given by $Q_W(Z, N) = Z(1 - 4\sin^2\theta_W) - N$, so, in the case of ^{12}C , it becomes proportional to the sine squared of the weak mixing angle [27]: $Q_W(6, 6) = -24\sin^2\theta_W$.

Given that the interaction of the electron with the nucleus involves only the conserved hadronic vector current, the “correction” term Δ in Eq. (2) vanishes at $Q^2 = 0$. However, nuclear and hadronic structures contribute to Δ at non zero Q^2 . Indeed, to leading order in α ,

$$\Delta \equiv F_{\text{wk}}(Q^2)/F_{\text{ch}}(Q^2) - 1 \quad (3)$$

is given by the ratio of the weak F_{wk} to the charge form factor F_{ch} . Both form factors are normalized to unity at $Q^2 = 0$. Each of the form factors is related to the corresponding spatial distributions of charge by a three-dimensional Fourier transform,

$$F(Q^2) = \int \rho(r) e^{i\mathbf{q}\cdot\mathbf{r}} d^3r, \quad \text{with } |\mathbf{q}| \equiv \sqrt{Q^2}. \quad (4)$$

Note that the normalization of the form factor at $Q^2 = 0$ implies that $\int \rho(r) d^3r = 1$. At low Q^2 , the form factors may be expanded in terms of various moments of their spatial distribution,

$$F(Q^2) = 1 - \frac{Q^2}{3!} \langle r^2 \rangle + \frac{Q^4}{5!} \langle r^4 \rangle + \mathcal{O}(Q^6), \quad (5)$$

where the second term defines the root-mean-square radius of the spatial distribution, namely,

$$R^2 \equiv \langle r^2 \rangle = \int r^2 \rho(r) d^3r. \quad (6)$$

Thus, to lowest order in Q^2 , Δ is proportional to the weak skin of the nucleus,

$$\Delta = -\frac{Q^2}{3} R_{\text{wskin}} R_{\text{ch}} + \mathcal{O}(Q^2 R_{\text{wskin}}^2). \quad (7)$$

The weak skin $R_{\text{wskin}} \equiv R_{\text{wk}} - R_{\text{ch}}$, or, equivalently,

$$\lambda = \frac{R_{\text{wk}} - R_{\text{ch}}}{R_{\text{ch}}} \quad (8)$$

coincides with the neutron skin in the idealized nonrelativistic picture, but is distinct from it once the small weak charge of the proton, relativistic effects, including strangeness, and radiative corrections are taken into account.

Two terms in Eq. (2) are of great interest: the weak mixing angle θ_W encoded in the weak charge [11, 17] and the ratio of nuclear form factors appearing in Δ ; to access the former, one must constrain the latter. Conversely, to extract nucleon- or nuclear-structure information from PVES, such as the strange quark content of the nucleon [26] or the weak skin of heavy nuclei [23], one assumes that Q_W is precisely known, so the measurement provides a constraint on Δ . In this Rapid Communication, we explore the possibility of a precise determination of both—the weak charge and the weak skin of ^{12}C —within one single experiment.

The P2 experimental program at the MESA facility in Mainz [17] includes a plan aiming for a 0.3% determination of the weak charge of ^{12}C . Given this ambitious goal, the tree-level formula of Eq. (7)—even when including higher-order terms in the Q^2 expansion—is not accurate enough. Order- α radiative corrections, particularly Coulomb distortions which scale as $Z\alpha$, should be included. To properly account for Coulomb distortions, we follow the formalism developed by one of us in Ref. [28]. The electron wave function Ψ satisfies the Dirac equation

$$\left(\boldsymbol{\alpha} \cdot \mathbf{p} + \beta m + V(r) + \gamma_5 A(r) \right) \Psi(\mathbf{r}) = E \Psi(\mathbf{r}), \quad (9)$$

where m is the electron mass, $\boldsymbol{\alpha}$, β , and γ_5 are Dirac matrices, and $V(r)$ and $A(r)$ are the vector (Coulomb) and axial-vector components of the potential, respectively [28]. Here, E stands for the electron energy in

the center-of-mass frame [29] which is related (neglecting the electron mass) to the laboratory energy E_{beam} by $E_{\text{beam}}/E = \sqrt{1+2E_{\text{beam}}/M}$ with M the nuclear mass.

The Coulomb potential is computed from the experimentally known nuclear charge distribution via

$$V(r) = -Z\alpha \int \frac{\rho_{\text{ch}}(r')}{|\mathbf{r} - \mathbf{r}'|} d^3r'. \quad (10)$$

The axial-vector potential for a point like weak charge is short-range $A(r) \propto \delta^3(\mathbf{r})$, but acquires a finite range due to the finite size of the nuclear weak charge distribution. That is,

$$A(r) = \frac{G_F Q_W}{2\sqrt{2}} \rho_{\text{wk}}(r). \quad (11)$$

The Dirac equation displayed in Eq. (9) is solved numerically using the ELSEPA package [30], properly modified to include the axial-vector potential [31, 32]. The intrinsic relative precision of the computation of A^{PV} is on the order of $10^{-4} - 10^{-5}$, and in a calculation at the per mille level there are only genuine uncertainties of ρ_{wk} itself.

For the nuclear charge distribution of ^{12}C , we use the parametrization of the world data on elastic electron-carbon scattering in the form of a sum of Gaussians [33]. The fact that the charge density of ^{12}C and its charge radius $R_{\text{ch}} = 2.4702(22)$ fm [34] are known with high precision serves as the basis for an accurate extraction of $\sin^2 \theta_W$ and of R_{wk} from a measured A^{PV} . A possible avenue is to rely on models to produce a range of predictions for ρ_{wk} which is then used to directly fit the PV asymmetry to determine the value of the weak radius as was performed in the case of the PREX. One choice for parametrizing the weak charge distribution is the two-parameter symmetrized Fermi distribution,

$$\rho_{\text{wk}}(r) = \rho_{\text{SF}}(r, c, a) = \rho_0 \frac{\sinh(c/a)}{\cosh(r/a) + \cosh(c/a)},$$

$$\rho_0 = \frac{3}{4\pi c(c^2 + \pi^2 a^2)}, \quad (12)$$

with c and a as the half-density radius and surface diffuseness, respectively, and ρ_{SF} is normalized to unity. The advantage of the symmetrized Fermi parametrization, apart from its simplicity, is that its form factor, and all of its moments are known analytically [35]. In particular, the mean-square radius of the distribution is

$$R_{\text{SF}}^2 = \frac{3}{5}c^2 + \frac{7}{5}\pi^2 a^2. \quad (13)$$

In Fig. 2, we show results for the PV asymmetry at a fixed electron beam energy of $E_{\text{beam}} = 155$ MeV as a function of the laboratory scattering angle θ and momentum transfer q . Results are displayed in both a plane-wave (tree-level) approximation and with Coulomb distortions. The two distorted-wave calculations use $\rho_{\text{wk}} = \rho_{\text{ch}}$ (no skin) and $\rho_{\text{wk}} = \rho_{\text{SF}}(r, c = 2.07 \text{ fm}, a = 0.494 \text{ fm})$ with

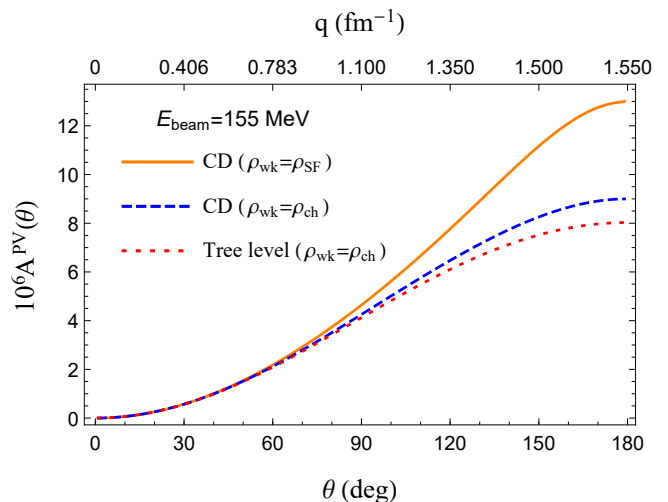


FIG. 2. The PV asymmetry for elastic electron scattering off ^{12}C at $E_{\text{beam}} = 155$ MeV as a function of the scattering angle θ (lower x axis) and of the momentum transfer $q = \sqrt{Q^2}$ (upper x axis). We show the plane-wave (tree-level) result with $\rho_{\text{wk}} = \rho_{\text{ch}}$ (red dotted curve) and the Coulomb distorted (CD) predictions with $\rho_{\text{wk}} = \rho_{\text{ch}}$ (blue dotted curve) and with $\rho_{\text{wk}} = \rho_{\text{SF}}(r, c = 2.07 \text{ fm}, a = 0.494 \text{ fm})$ (solid orange curve).

$R_{\text{wk}} = 2.44$ fm which falls within the range of values of a representative set of nuclear-structure models [36–38]. We observe a strong dependence of the PV asymmetry on the value of the weak skin, especially at backward angles. We also find that it is important to include effects due to Coulomb distortions. Our results displayed in Fig. 2 are qualitatively similar to those obtained in Ref. [39], but a quantitative comparison is difficult because of different perspectives adopted in the calculation of the weak charge density, and several kinematic approximations used in that paper.

Unfortunately, the choice of a particular form for the weak charge distribution introduces model dependence that may be difficult to quantify when extracting weak charge and radius from a measurement of A^{PV} : models that predict different values for the weak radius would generally differ in all the higher moments of the weak charge distribution, as well. To unambiguously disentangle the effect of the weak skin, we propose a different method. Given the $N = Z$ character of ^{12}C , its weak charge distribution is expected to follow closely the electric charge distribution. We introduce the small difference between the two, the “weak-skin” distribution,

$$\rho_{\text{wskin}}(r) \equiv \rho_{\text{wk}}(r) - \rho_{\text{ch}}(r). \quad (14)$$

Note that ρ_{wskin} is the spatial analog of the weak-skin form factor depicted in Figs. 3 and 6 of Ref. [20]. $\rho_{\text{wskin}}(r)$ is normalized to zero and its second moment can be fixed to

$$\int \rho_{\text{wskin}}(r) r^2 d^3r = R_{\text{wk}}^2 - R_{\text{ch}}^2 = 2\lambda R_{\text{ch}}^2 + \mathcal{O}(\lambda^2). \quad (15)$$

This allows us to write

$$\rho_{\text{wskin}}(r) = \lambda \bar{\rho}(r; \zeta), \quad (16)$$

where ζ is representative of the model dependence. This parametrization is advantageous because it allows to explicitly separate the dependence on λ from the effects of the higher moments of the weak charge density encapsulated in a (set of) model parameter(s) ζ . For example, assuming the symmetrized Fermi parametrization of ρ_{wk} as in Eq. (12), one would find

$$\rho_{\text{wskin}}(r) = (\lambda/\lambda_{\text{SF}}) \left(\rho_{\text{SF}}(r, c, a) - \rho_{\text{ch}}(r) \right) \quad (17)$$

with $\lambda_{\text{SF}} = \lambda_{\text{SF}}(c, a) = R_{\text{SF}}(c, a)/R_{\text{ch}} - 1$.

This parametrization corresponds to rewriting Δ in Eq. (3) as

$$\begin{aligned} \Delta &= -\frac{\lambda}{3} Q^2 R_{\text{ch}}^2 + \left(\frac{F_{\text{wk}}}{F_{\text{ch}}} - 1 + \frac{\lambda}{3} Q^2 R_{\text{ch}}^2 \right) \\ &= -\frac{\lambda}{3} Q^2 R_{\text{ch}}^2 + \left[\frac{\lambda}{\lambda_{\text{SF}}} \left(\frac{F_{\text{SF}}}{F_{\text{ch}}} - 1 \right) + \frac{\lambda}{3} Q^2 R_{\text{ch}}^2 \right], \end{aligned} \quad (18)$$

and the low- Q^2 expansion of the term in the square brackets starts at the order Q^4 by construction. The nuclear models [36–38] are used here—not to predict the distribution of weak charge in ^{12}C , but rather—to determine the range of values that need to be explored to quantify the uncertainty in Δ . These models, all informed by the charge radii and binding energies of a variety of nuclei including ^{12}C , predict $|\lambda_{\text{SF}}| \lesssim 2\%$ with the central value of $\lambda_0 = -0.90\%$.

To address the possibility to determine the weak charge of ^{12}C with a precision of 0.3% in the P2 experiment, we study the sensitivity of the PV asymmetry to nuclear-structure uncertainties. In Fig. 3, we display results for A^{PV} as a function of λ for an incident electron energy of $E_{\text{beam}} = 155$ MeV and two fixed scattering angles: $\theta = 29^\circ$ (upper panel) and $\theta = 145^\circ$ (lower panel). The blue band corresponds to λ varying in the range suggested by the models. Its width indicates the spread of model predictions for F_{wk} and the central line is the bisector of the predictions for the extreme choices of the models. The pink-shaded band in the $\theta = 29^\circ$ plot indicates the anticipated 0.3% precision in A^{PV} . From the sensitivity of the forward angle measurement to λ shown in Fig. 3, one concludes that λ should be known with a precision of 0.6% or better to constrain the weak charge of ^{12}C to about 0.3%. Given that the nuclear models suggest a larger uncertainty in λ , we conclude that with a single measurement and theory input alone this task is not feasible.

Another option is to employ a second measurement of A^{PV} at 145° (the lower panel of Fig. 3) to constrain the value of λ to a narrower range. It is seen that varying λ in the adopted range translates into a $\pm 24\%$ variation in the asymmetry. Hence, a measurement at this backward

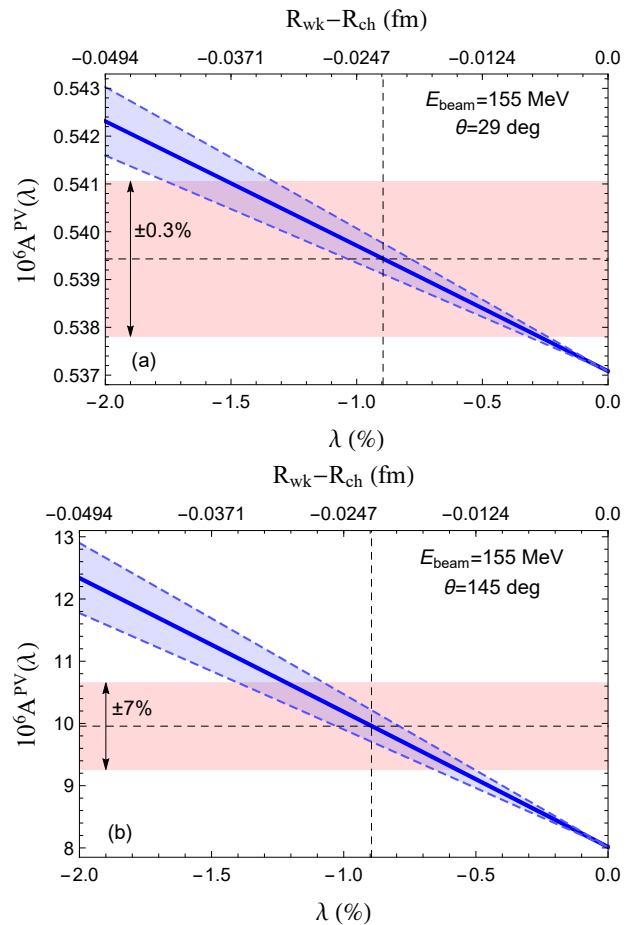


FIG. 3. The PV asymmetry at P2 with $E_{\text{beam}} = 155$ MeV for the (a) forward ($\theta = 29^\circ$) and (b) backward measurement ($\theta = 145^\circ$) as a function of the skin parameter λ . The pink-shaded band in the $\theta = 29^\circ$ ($\theta = 145^\circ$) plot indicates the anticipated (suggested) 0.3% (7%) precision in A^{PV} . The blue band describes the residual model dependence as explained in the text. The vertical and horizontal dashed lines correspond to $\lambda = \lambda_0$ and $A^{\text{PV}}(\lambda) = A^{\text{PV}}(\lambda_0)$, respectively.

kinematical setting with a higher precision will reduce the range of values of λ and ultimately guarantee a precise extraction of the weak mixing angle from a combination of the two measurements. To a very good approximation the λ -dependence of A^{PV} seen in Fig. 3 is linear, and we can write

$$A^{\text{PV}} = -\frac{G_F Q^2}{4\sqrt{2}\pi\alpha} \frac{Q_W}{Z} \left(1 + p_0 + (p_1 + p_2 \zeta) \lambda \right), \quad (19)$$

so that the effect of varying ζ is depicted by the blue bands in Fig. 3. The parameter ζ can be chosen in such a way that $\zeta = \zeta_0 = 0$ corresponds to the central prediction and $\zeta = \pm 1$ to the upper and lower limits of the error band. Results of the distorted-wave calculation of the coefficients p_0 , p_1 , and p_2 are provided in Supplemental Material.

We perform a χ^2 fit of the combined forward (A_f^{PV})

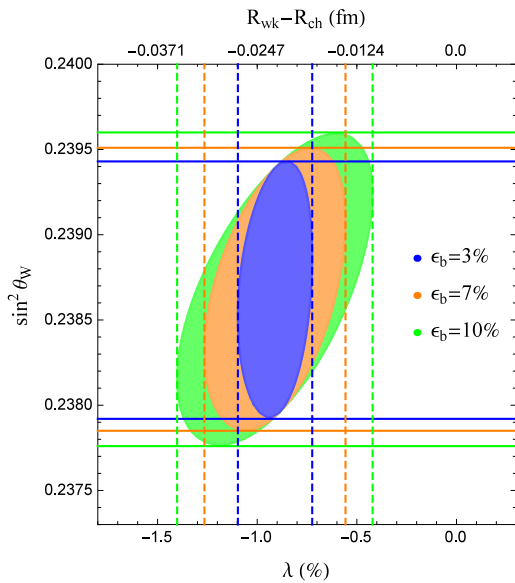


FIG. 4. The 1σ -error regions from a fit of two expected measurements at forward and backward angles to the weak mixing angle, the skin parameter λ and the model parameter ζ . The plot shows the projection onto the $\sin^2\theta_W$ - λ -plane. The green, orange and blue ellipses correspond to three assumptions for the precision ϵ_b of the backward measurement (10%, 7%, and 3%) whereas the precision of the forward measurement was always assumed to be 0.3%.

and backward (A_b^{PV}) measurements with respect to the three free parameters $\sin^2\theta_W$, λ and ζ . That is,

$$\chi^2(\sin^2\theta_W, \lambda, \zeta) = \sum_{i=f,b} \left(\frac{A_i^{\text{exp}} - A_i^{\text{PV}}(\sin^2\theta_W, \lambda, \zeta)}{\delta A_i} \right)^2 + \left(\frac{\zeta - \zeta_0}{\delta\zeta} \right)^2. \quad (20)$$

We assume that the experimental values of A_i^{exp} agree with the SM prediction for which we choose the central value of $\lambda = \lambda_0$. The experimental uncertainties are given by δA_i . The last term in Eq. (20) encodes our biases for the expected range of values of ζ , and we have chosen $\delta\zeta = 1$. The 1σ -allowed range for $\sin^2\theta_W$ and λ is obtained by solving $\chi^2(\sin^2\theta_W, \lambda, \zeta) = 1$. In Fig. 4 we show the projection of the $\chi^2 = 1$ solution onto the $\sin^2\theta_W$ - λ plane for three different choices of the precision of the backward-angle measurement. The accuracy of the forward measurement remains fixed at 0.3%. The covariance ellipses in Fig. 4 suggest that $\sin^2\theta_W$ and λ are correlated and their correlation decreases with increasing accuracy of the backward measurement. Moreover, fractional uncertainties are given by: $\delta\sin^2\theta_W/\sin^2\theta_W = \pm 0.39\%$ for $\delta A_b/A_b^{\text{PV}} = 10\%$ and $\delta\sin^2\theta_W/\sin^2\theta_W = \pm 0.35\%$ for $\delta A_b/A_b^{\text{PV}} = 7\%$. An even higher precision of the backward measurement, 3%, results in a reduction in the uncertainty of the weak mixing angle to $\delta\sin^2\theta_W/\sin^2\theta_W = \pm 0.32\%$. At this point the uncertainty starts being dominated by the forward

measurement, so further improvement to the backward measurement has no impact on the precision of $\sin^2\theta_W$.

To summarize, we presented an ambitious proposal for a simultaneous sub percent determination of the weak charge and weak radius of ^{12}C using parity-violating electron scattering at the upcoming MESA facility in Mainz. We demonstrated that to take full advantage of an unprecedented 0.3% precision aimed for in the forward kinematical setting of P2 [17], an additional 3–7% measurement at a backward angle of 145° will ensure a largely model-independent extraction of $\sin^2\theta_W$ with a relative precision of 0.32–0.35% and determination of R_{wk} within 0.19–0.35% of R_{ch} . Note that a similar combination of forward and backward measurements on the proton is planned as part of the P2 experiment [17], which makes the proposal presented in this Rapid Communication a viable and attractive possibility.

Whereas the weak skin of ^{12}C and other symmetric nuclei does not constrain the nuclear EOS, its exact value will help quantifying generic isospin symmetry-breaking (ISB) effects. Coulomb repulsion among the protons inside a nucleus and other ISB mechanisms lead to a mismatch in the distribution of neutrons and protons therein. Along with generating the proton (and weak) skin of symmetric nuclei, ISB contributions play a major role in the analysis of superallowed nuclear β decays and the extraction of V_{ud} [40]. Importantly, in all pairs of nuclei involved in the known superallowed β transitions, either the parent or the daughter nucleus is symmetric. Therefore, precise information on weak skins of the (nearly) symmetric parent and daughter nuclei will have an impact on the tests of unitarity of the Cabibbo-Kobayashi-Maskawa matrix and new physics searches with superallowed nuclear β decays.

Acknowledgments – The authors acknowledge useful discussions with K. Kumar and F. Maas. We thank T. W. Donnelly, R. Ferro-Hernández, and O. Moreno for helpful correspondence. The work of J. E., M. G., O. K., and H. S. was supported by the German-Mexican Research Collaboration Grants No. 278017 (CONACyT) and No. SP 778/4-1 (DFG). M. G. was supported by the EU Horizon 2020 Research and Innovation Programme, Project No. STRONG-2020, Grant Agreement No. 824093. X. R.-M. acknowledges funding from the EU Horizon 2020 research and innovation programme, grant agreement No. 654002. J. P. acknowledges support from the U.S. Department of Energy Office of Nuclear Physics under Award No. DE-FG02-92ER40750. C.-Y. S. was supported, in part, by the DFG (Grant No. TRR110) and the NSFC (Grant No. 11621131001) through the funds provided to the Sino-German CRC 110 “Symmetries and the Emergence of Structure in QCD,” and by the Alexander von Humboldt Foundation through the Humboldt Research Fellowship. C. J. H. was supported by the U. S. Department of Energy Grants No. DE-FG02-87ER40365 and No. DE-SC0018083.

SUPPLEMENTAL MATERIAL

1. In Table I we provide parameters of nuclear models used in our calculation of the parity-violating asymmetry and parameters ζ_f (ζ_b) determined as a result of the calculation which accounts for Coulomb distortion effects at forward (backward) scattering angles.

TABLE I.

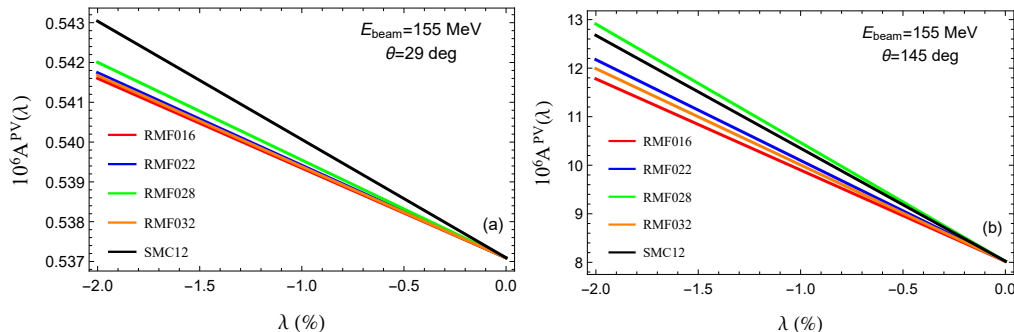
Model	c , fm	a , fm	R_{SF} , fm	λ_{SF} , %	ζ_f	ζ_b
RMF016	2.06065	0.49389	2.43274	-1.52	-1.00	-1.00
RMF022	2.06849	0.49445	2.43830	-1.29	-0.80	-0.30
RMF028	2.07585	0.49544	2.44482	-1.03	-0.44	+1.00
RMF032	2.06421	0.49433	2.43578	-1.39	-0.89	-0.62
SMC12	2.22693	0.47318	2.46358	-0.27	+1.00	+0.59

The first four models listed in Table I fall under the general rubric of covariant (or relativistic) energy density functionals. The models are based on an underlying Lagrangian density that includes nucleons interacting via the exchange of various mesons and the photon. In addition, nonlinear meson interactions are included to account for many-body forces. The calibration of the handful of model parameters is informed by ground-state properties of finite nuclei, their collective response, and constraints on the maximum neutron-star mass [36]. Incorporated in the ground state properties are charge radii of a variety of magic and semi-magic nuclei, including ^{12}C . The outcome of the calibration procedure is an optimal set of parameters together with a covariance matrix that properly accounts for statistical uncertainties and correlations. The fitting protocol for all the models is identical save one important distinction: the assumed value for the yet to be determined neutron skin thickness of ^{208}Pb (R_{skin}^{208}). Indeed, the neutron skin thickness of ^{208}Pb is allowed to vary over the range of $R_{\text{skin}}^{208} = (0.16 - 0.32)$ fm [37].

The model named SMC12 is a non-relativistic energy density functional of the Skyrme type. SMC12 has been devised to reproduce the binding energy (B) and charge radii (R_{ch}) of ^{12}C without compromising the accuracy in the description of other observables along the nuclear chart. Specifically, the fitting protocol has been based on that of the SAMi interaction [38] with the following modifications: i) inclusion of ^{12}C data (B and R_{ch}); and ii) relaxation of the weight on the pure neutron matter equation of state. This allowed us to accommodate the new data within the presented model. As an example, the experimental charge radii and nuclear masses of ^{12}C , ^{16}O , ^{40}Ca , ^{48}Ca , ^{90}Zr , and ^{208}Pb are reproduced to better than 1% accuracy, except for the binding energy of the two Calcium isotopes which are accurate at the percent level. This example justifies the reliability of the model for the present study.

To sum up, the five models that we selected for our analysis cover a fairly wide landscape in the parameter space. For the energy density functionals that we used, the predicted neutron skin thickness of ^{208}Pb ranges from about 0.12 fm all the way to 0.32 fm; going beyond this range is hard without compromising the agreement with experiment.

2. In Fig. 5 we present an example of the calculation which accounts for Coulomb distortion effects at forward ($\theta = 29^\circ$) and backward ($\theta = 145^\circ$) scattering angles.

FIG. 5. Predictions for A^{PV} at (a) $\theta = 29^\circ$ and (b) $\theta = 145^\circ$.

3. In Table II we provide the coefficients p_0 , p_1 , and p_2 obtained as a result of the calculation which accounts for Coulomb distortion effects at forward and backward scattering angles. These coefficients are defined by Eq. (19).

TABLE II.

Coefficient	$\theta = 29^\circ$	$\theta = 145^\circ$
p_0	+0.04005	+0.09586
p_1	-0.50612	-29.5132
p_2	-0.06969	-3.86420

* koshchii@uni-mainz.de

- [1] S. Schael *et al.* [ALEPH and DELPHI and L3 and OPAL and SLD Collaborations and LEP Electroweak Working Group and SLD Electroweak Group and SLD Heavy Flavour Group], Precision electroweak measurements on the Z resonance, Phys. Rept. **427** (2006) 257.
- [2] T. A. Aaltonen *et al.* [CDF and D0 Collaborations], Tevatron Run II combination of the effective leptonic electroweak mixing angle, Phys. Rev. D **97** (2018), 112007.
- [3] R. Aaij *et al.* [LHCb Collaboration], Measurement of the forward-backward asymmetry in $Z/\gamma^* \rightarrow \mu^+\mu^-$ decays and determination of the effective weak mixing angle, JHEP **1511** (2015) 190.
- [4] ATLAS Collaboration, Measurement of the effective leptonic weak mixing angle using electron and muon pairs from Z -boson decay in the ATLAS experiment at $\sqrt{s} = 8$ TeV, Tech. Rep. ATLAS-CONF-2018-037, CERN (2018).
- [5] A. M. Sirunyan *et al.* [CMS Collaboration], Measurement of the weak mixing angle using the forward-backward asymmetry of Drell-Yan events in pp collisions at 8 TeV, Eur. Phys. J. C **78** (2018) 701.
- [6] C. Y. Prescott *et al.*, Further Measurements of Parity Nonconservation in Inelastic electron Scattering, Phys. Lett. **84B**, 524 (1979).
- [7] D. Wang *et al.* [PVDIS Collaboration], Measurement of parity violation in electronquark scattering, Nature **506**, no. 7486, 67 (2014).
- [8] G. P. Zeller *et al.* [NuTeV Collaboration], A Precise Determination of Electroweak Parameters in Neutrino Nucleon Scattering, Phys. Rev. Lett. **88** (2002) 091802; Erratum: [Phys. Rev. Lett. **90** (2003) 239902(E).]
- [9] C. S. Wood, S. C. Bennett, D. Cho, B. P. Masterson, J. L. Roberts, C. E. Tanner and C. E. Wieman, Measurement of parity nonconservation and an anapole moment in cesium, Science **275**, 1759 (1997).
- [10] J. Guena, M. Lintz and M. A. Bouchiat, Measurement of the parity violating $6S$ - $7S$ transition amplitude in cesium achieved within 2×10^{-13} atomic-unit accuracy by stimulated-emission detection, Phys. Rev. A **71** (2005) 042108.
- [11] D. Androić *et al.* [Qweak Collaboration], Precision measurement of the weak charge of the proton, Nature **557**, no. 7704, 207 (2018).
- [12] P. L. Anthony *et al.* [SLAC E158 Collaboration], Precision measurement of the weak mixing angle in Moller scattering, Phys. Rev. Lett. **95** (2005) 081601.
- [13] J. Erler and M. J. Ramsey-Musolf, The Weak mixing angle at low energies, Phys. Rev. D **72**, 073003 (2005).
- [14] J. Erler and R. Ferro-Hernández, Weak Mixing Angle in the Thomson Limit, JHEP **1803**, 196 (2018).
- [15] J. Zhang *et al.*, Efficient inter-trap transfer of cold francium atoms, Hyperfine Interact. **237** (2016) 150.
- [16] D. Antypas, A. Fabricant, J. E. Stalnaker, K. Tsigitkin, V. V. Flambaum and D. Budker, Isotopic variation of parity violation in atomic ytterbium, Nature Phys. **15** (2019) 120.
- [17] D. Becker *et al.*, The P2 experiment, Eur. Phys. J. A **54** (2018) 208.
- [18] J. Benesch *et al.* [MOLLER Collaboration], The MOLLER Experiment: An Ultra-Precise Measurement of the Weak Mixing Angle Using Møller Scattering, arXiv:1411.4088 [nucl-ex].
- [19] P. A. Souder, Parity Violation in Deep Inelastic Scattering with the SoLID Spectrometer at JLab, Int. J. Mod. Phys. Conf. Ser. **40**, 1660077 (2016).
- [20] M. Thiel, C. Sienti, J. Piekarewicz, C. J. Horowitz and M. Vanderhaeghen, Neutron skins of atomic nuclei: per aspera ad astra, J. Phys. G **46** (2019) 093003.
- [21] C. J. Horowitz and J. Piekarewicz, Neutron Star Structure and the Neutron Radius of ^{208}Pb , Phys. Rev. Lett. **86** (2001) 5647.
- [22] S. Abrahamyan *et al.*, Measurement of the Neutron Radius of ^{208}Pb through Parity Violation in Electron Scattering, Phys. Rev. Lett. **108** (2012) 112502.
- [23] C. J. Horowitz *et al.*, Weak charge form factor and radius of ^{208}Pb through parity violation in electron scattering, Phys. Rev. C **85** (2012) 032501(R).
- [24] K. Paschke *et al.*, PREX-II: Precision parity-violating measurement of the neutron skin of lead. <http://hallaweb.jlab.org/parity/prex/prexII.pdf>, Proposal to Jefferson Lab PAC 38, 2011.
- [25] J. Mammei *et al.* [CREX collaboration], Parity-violating measurement of the weak charge distribution of Ca to 0.02 fm accuracy. http://hallaweb.jlab.org/parity/prex/c-rex2013_v7.pdf, Proposal to Jefferson Lab PAC 40, 2013.
- [26] F. E. Maas and K. D. Paschke, Strange nucleon form-

- factors, *Prog. Part. Nucl. Phys.* **95** (2017) 209.
- [27] The discussion of electroweak radiative corrections is deferred to a future work.
- [28] C. J. Horowitz, Parity violating elastic electron scattering and Coulomb distortions, *Phys. Rev. C* **57** (1998) 3430.
- [29] Other choices of the reference frame would introduce corrections depending on the nuclear recoil. Up to now, no fully consistent way of accounting for recoil corrections in the Dirac formalism is known.
- [30] F. Salvat, A. Jablonski, C. J. Powell, ELSEPA — Dirac partial-wave calculation of elastic scattering of electrons and positrons by atoms, positive ions and molecules, *Comp. Phys. Comm.* **165** (2005) 157.
- [31] X. Roca-Maza, M. Centelles, X. Viñas, and M. Warda, Neutron Skin of ^{208}Pb , Nuclear Symmetry Energy, and the Parity Radius Experiment, *Phys. Rev. Lett.* **106**, (2011) 252501.
- [32] O. Koshchii et al., to be published.
- [33] H. De Vries, C. W. De Jager and C. De Vries, Nuclear charge and magnetization density distribution parameters from elastic electron scattering, *Atom. Data Nucl. Data Tabl.* **36** (1987) 495.
- [34] I. Angeli and K.P. Marinova, Table of experimental nuclear ground state charge radii: An update, *Atom. Data Nucl. Data Tabl.* **99** (2013) 69.
- [35] J. Piekarewicz, A. R. Linero, P. Giuliani and E. Chicken, Power of two: Assessing the impact of a second measurement of the weak-charge form factor of ^{208}Pb , *Phys. Rev. C* **94**, 034316 (2016).
- [36] W.-C. Chen and J. Piekarewicz, Building relativistic mean field models for finite nuclei and neutron stars, *Phys. Rev. C* **90** (2014) 044305.
- [37] W.-C. Chen and J. Piekarewicz, Searching for isovector signatures in the neutron-rich oxygen and calcium isotopes, *Phys. Lett. B* **748** (2015) 284.
- [38] X. Roca-Maza, G Colò and H. Sagawa, A new Skyrme interaction with improved spin-isospin properties, *Phys. Rev. C* **86** (2012) 031306.
- [39] O. Moreno and T. W. Donnelly, Nuclear structure uncertainties in parity-violating electron scattering from ^{12}C , *Phys. Rev. C* **89**, 015501 (2014).
- [40] J. C. Hardy and I. S. Towner, Superallowed $0^+ \rightarrow 0^+$ nuclear β decays: 2014 critical survey, with precise results for V_{ud} and CKM unitarity, *Phys. Rev. C* **91** (2015), 025501.